Atmos. Meas. Tech. Discuss., https://doi.org/10.5194/amt-2017-132
Manuscript under review for journal Atmos. Meas. Tech.
Discussion started: 9 June 2017

Atmospheric Measurement Techniques Discussions

Impact of pitch angle fluctuations on airborne lidar sensing ahead along the flight direction

Alexander Sergeevich Gurvich [1] and Victor Alexeevich Kulikov [1,2]

[1]Obukhov Institute of Atmospheric Physics, Russian Academy of Science, 3 Pyzhevskii pereulok str., Moscow, Russia, 119017
[2]University of Dayton, 300 College Park, Dayton, OH, USA 45469

Correspondence to: Victor A. Kulikov (victoralexkulikov@gmail.com)

Abstract. Airborne lidar sensing ahead along the flight direction can serve for notification of clear air turbulence (CAT) and help to prevent injuries or fatal air accidents. The validation of this concept was presented in the framework of the DELICAT (DEmonstration of LIdar based CAT detection) project. However, the difficulties encountered during the processing of DELICAT data indicated the need of a better understanding the observational errors due to geometrical factors. In this paper, we discuss possible error sources imminent to this technique, related to fluctuations of the flight parameters, which may lead to an incorrect estimation of the turbulence intensity. We analyze the variations of backscattered lidar signal caused by fluctuations of the most important ahead sensing flight parameter, the pitch angle. The fluctuation values considered in the paper correspond to the error limits of the compensational gyro-platform used in the civil aviation. Uncompensated pitch angle fluctuations in the presence of aerosol concentration variations can lead to noticeable signal variations that can be mistakenly attributed to wind shear, turbulence or fast evolution of aerosol layer. We formulate the criteria that allow the recognition of signal variations caused by pitch angle fluctuations. Influence of these fluctuations is shown to be stronger for aerosol variations on smaller vertical scales. An example of DELICAT observations indicating a noticeable pitch angle fluctuation impact is presented.

1 Introduction

Airborne lidar systems (Fukuchi and Shiina, 2012; Weitkamp, 2006) may play a significant role in alarming, preventing, and compensating problems caused by atmospheric turbulence. Such system were previously devloped for short range sounding (Schmitt et al., 2007; Jentink and Bogue, 2005). Recently, a medium range lidar was developed, built and tested in the framework of the DELICAT (DEmonstration of LIdar based Clear Air Turbulence detection) (Huffaker and Hardesty, 1996; Inokuchi et al., 2009; Veerman et al., 2014; Gurvich and Kulikov, 2013; Inokuchi et al., 2009b; Targ et al., 1996; Thales Avionics and ONERA, 2004). Medium range systems are focused on 20-30 km sensing distance, which corresponds to 2–10 minutes of warning time for typical flight speed of airplane and helicopter correspondingly. An earlier warning is preferable and airborne lidar with larger sensing distance could be developed in a future.

Sensing of turbulence can be based on backscattered signal from air density fluctuations (Veerman et al., 2014) which allows detecting turbulence even in the absence of scatterers. At the same time, dust and smog, water vapor etc. contribute to the

Atmos. Meas. Tech. Discuss., https://doi.org/10.5194/amt-2017-132
Manuscript under review for journal Atmos. Meas. Tech.
Discussion started: 9 June 2017

Atmospheric Measurement Techniques Discussions

backscattered signal as well. The signal filtration is a good method to exclude undesirable contributions (Hair et al., 2008) but it is impossible to cut responses from all types of atmospheric aerosol. Backscattered signal measurements at different polarizations (Burton et al., 2015; Veerman et al., 2014) will only allow excluding the component produced by non-spherical aerosol particles. The measured signal is, however, composed of the responses of different atmospheric components. A signal at the background level should not be a problem for turbulence detection even in presence of aerosol. The problem arises when the signal from aerosol layers is changing during the observation time.

A series of atmospheric processes influence the aerosol concentration and turbulence strength on temporal and spatial scales of medium range sensing. The aerosol concentration can change due to wind shear and evaporation/condensation processes (Ivlev and Dovgalyuk, 1999). For example, small cloud with horizontal characteristic scales about one kilometer can be displaced completely out of originally occupied volume during 40–200 sec by the wind with a speed within the range of 5–25 m/s (Liu et al., 2002). Clouds, as well as significant concentration changes in the could split into numerous small clusters at the horizontal scale of one or several kilometers were observed for different types of aerosol (Chazette et al., 2012; Cadet et al., 2005; Reichardt et al., 2002). The concentrations of both submicron aerosol and gas may change by 2–3 times during the equilibration process at characteristic time scales of about 3 minutes (Meng and Seinfeld, 1996). Gravity waves (Nappo, 2013; Fritts and Alexander, 2003) also impact clear air turbulence (CAT) (Plougonven and Zhang, 2016; Lane et al., 2003), especially at scales of about 700 m (Koch et al., 2005). The smallest spatial and temporal scales of gravity waves amount to about 1 km and 1-2 minutes, respectively (Lu and Koch, 2008; Koch et al., 2005; Plougonven and Zhang, 2016). Therefore, lidar sensing ahead along the flight direction does not only allow the operational detection of dangerous atmospheric conditions but can also provide information on macrostructures in the aerosol spatiotemporal distribution. At the same time, the signal variations at this time scale may be caused by the variations of lidar sensing trajectory due to the fluctuations of the flight parameters.

Backscattered signal can also be influenced by changing laser pulse properties or atmospheric propagation effects. Laser instability leads to time variation of both power and shape of pulses, which results in the change of the backscattered signal. Multipath propagation effect is usually ignored in consideration of backscattered signal, which can significantly degrade the accuracy of the measurement analysis (Godbaz et al., 2012). Strong laser pulses may indicate a non-linear interaction with the medium, resulting in the filamentation effect (Kosareva et al., 2006; Kandidov et al., 2009). The detectors can be a source of noise, which depends on the input signal (Acharya et al., 2004). These factors also contribute to the complexity of the signal analysis.

In this paper, we discuss the source of errors, which is specific to the airborne measurements. Variations of aircraft flight height and direction angle are always present in airborne measurements and they influence the observed backscattered signal. Uncontrolled fluctuations of flight height are usually about several meters and lead to the same height shift along the sensing path. It is highly probable that atmospheric aerosol and turbulence properties do not changes noticeably at the scale of a few meters. Variations of flight direction angle lead to variations of the sensing pulse trajectory. Variations of sensing angles for lidars mounted on gyro-platform should be within the error limits of these compensating systems. The accuracy of pitch angle measurements and fluctuation compensation is about 0.1–0.2 degree rms (SOMAG AG Jena, 2016; Temp-Avia, 2016). Thus the uncompensated angles lie in the range of 0.3–0.6 degrees, which corresponds to 150–300 m shift at the end of a 30 km

Atmos. Meas. Tech. Discuss., https://doi.org/10.5194/amt-2017-132
Manuscript under review for journal Atmos. Meas. Tech.
Discussion started: 9 June 2017

Atmospheric Measurement Techniques Discussions

path. Roll and yaw angle fluctuations do not influence the backscattered signal because this shift is small as compared to the horizontal size of the smallest atmospheric clouds, which is about one kilometer and more. At the same time pitch angle fluctuation can result in significant signal variations, if the trajectory shift caused by the angular deviation and the horizontal characteristic scale of aerosol concentration changes are comparable.

There are many experimental observations of variations of aerosol and water vapor concentration on small vertical (about one hundred m) and horizontal (several km) scales in the lower atmosphere. Small clouds with such characteristic scales a referred to as “clusters”, in order to avoid mixing them up with usual aerosol layers and clouds with the horizontal length of the order of hundred kilometers. Clusters can be produced, for example, at the final stage of the collapse of internal gravity waves (Barenblatt and Monin, 1979) or by turbulence (Klyatskin, 2005; Klyatskin and Koshel, 2000).

Observations of Eyjafjallajokull volcano eruption in 2010 showed small cluster structures as well as huge ash clouds. In the observation carried out by Chazette et al. by Ultra-Violet Rayleigh-Mie lidar, clusters with minimal horizontal size corresponding to about 50 seconds of aircraft flight time and 80 meters thickness were found (Chazette et al., 2012, Fig.3, Fig 4). At the same time clouds with sizes up to 1 km in the vertical direction and 100 km in the horizontal direction were also observed (Chazette et al., 2012). Layers with 1 and 2 km thickness and concentration changes about 7 times at this scale were found in (Dacre et al., 2013, Fig.3). The same thickness with a concentration jump, which is 2 time smaller, was also found in (Turnbull et al., 2012). Simulations predict clouds with thickness about of 0.5–2 km (Hervo et al., 2012, (Fig.1)) when real observations also show thin layers with thickness of about 100 meters (Hervo et al., 2012, Fig.2, Fig.10).

Cirrus cloud split into numerous clusters with a thickness of about 100 meters at the altitudes between 6 and 11 km ((Reichardt et al., 2002),Fig.1 or (Cadet et al., 2005),Fig.2b) and stable layers with 1 km thickness ((Cadet et al., 2005),Fig.2a) were observed. Based on possible wind speed, the horizontal size of these clusters can be estimated as 3–12 km. Their concentration is changing 2–5 times in both vertical and horizontal directions at cluster scales. Ice clouds containing cluster structures with horizontal characteristic scales about hundred meters were observed, for example in ((Haarig et al., 2016), Fig.2) at altitudes about 7–11 km. Aerosol clusters in the altitude range of 1–10 km with the thickness of about 100 m and the concentration variations by 2–5 times were reported in (Burton et al., 2015, Fig.3), (Burton et al., 2014, Fig.6 dust aerosol), (Burton et al., 2015, Fig.7, Fig.13), (Burton et al., 2014, smoke aerosol in Fig.9). Clusters with the 100 meter thickness and horizontal size of about few kilometers were also observed in (Hair et al., 2008). Urban plumes measured in (Kleinman et al., 2008) also contained clusters with horizontal sizes correspondinf to about of 1-2 minutes of aircraft flight time with 4 times concentration changes.

Relatively thin and long water vapor layers observed at heights below 11 km indicate a thickness of about 100 meters and more (Whiteman et al., 1992; Kiemle et al., 2008; Leblanc and McDermid, 2008). An ice layer with 100 meters vertical size can have more than 10 times concentration changes (Johnson et al., 2012).

Aerosol and water vapor clusters can be routinely observed in the atmosphere in the civil aviation flight height range. The shear of cluster with horizontal characteristic scale of about 1 km at wind speed of 20 m/s could happen in about 30–60 seconds. The evaporation and condensation effects can also influence the time of aerosol cluster evolution. On the other hand, cluster

Atmos. Meas. Tech. Discuss., https://doi.org/10.5194/amt-2017-132
Manuscript under review for journal Atmos. Meas. Tech.
Discussion started: 9 June 2017

Atmospheric Measurement Techniques Discussions

could disappear from the field of view because of pitch angle fluctuation during the same time. This creates potential ambiguity in the interpretation of the lidar backscattering signal.

In this paper, we discuss the impact of pitch angle fluctuations on both simulated and measured lidar signal in the presence of aerosol clusters with different sizes monitored by an airborne lidar. We formulate the criteria for distinguishing of pitch angle fluctuation impact from the natural changes caused by wind or time evolution. The paper is organized as follows: in Sections 2 and 3, we describe the observation model and its parameters, respectively. The simulation results are presented and discussed in Section 4. In Section 5, we make our conclusions.

2 Observation model and typical scales

Ground-based stationary lidar is the conventional technique for the study of the atmospheric composition, density, and aerosol properties (Zuev and Zuev, 1992). The sensing procedure is as follows: short radiation pulses are produced sequentially by a pulsed laser, each of them is transformed into a narrow beam by the optical system and sent into the atmosphere. Thermodynamic fluctuations of air density (Fabelinskii, 2012) and particle concentration for solid or liquid aerosol (Bohren and Huffman, 2008) scatter the beam. Measured power profiles of the scattered radiation are a function of shot time t and distance L to the scattering volume, the latter being derived from measured backscatter delay time δt. For a ground-based lidar with an upwards-directed beam, L equals the altitude of the scattering volume and the power of the registered lidar response I bears information on the atmospheric properties along the line of sight (Hauchecorne et al., 2016; Keckhut et al., 2015). As the wind drift occurs, the altitudinal cross-section of long-living aerosol clusters can be inferred from $I(L,t)$ relief images in the (L,t) plane as bars with width depending on both the wind speed and the 3D cluster structure (Haarig et al., 2016; Hoareau et al., 2012).

The wind drift poses a significant encumbrance to studies of aerosol cluster evolution, using ground-based platforms, because it is necessary to distinguish between the temporal evolution of a particular cluster and its drift in space with the wind. While thermodynamic fluctuations of atmospheric air density in time and space may be described under the assumption of their statistical homogeneity and stationarity, this assumption, in practice, often becomes invalid for the description of clusterized aerosol.

For the enhancement of the civil aviation safety and flight comfort, it was suggested to use an air-borne lidar with scanning the atmosphere ahead in the flight direction. The analysis of experimental results presented in (Veerman et al., 2014, Fig. 22), suggests a rapid spatiotemporal evolution of aerosol clusters. A schematic diagram of lidar measurements that takes account of random pitch angle variations is shown in Fig.1. In field experiments, noise and distortions of the data are always present. One of the crucial factors is the noise related to uncontrolled fluctuations of the aircraft position and, as a result, of the airborne lidar position. In this work, we develop the results of a previous study (Gurvich and Kulikov, 2016), by the consideration of the spatiotemporal parameters of lidar images of aerosol clusters and by the assessment of the characteristic scales of clusters, at which noise caused by uncontrolled fluctuations of the aircraft position does not impede monitoring their evolution.

Atmos. Meas. Tech. Discuss., https://doi.org/10.5194/amt-2017-132
Manuscript under review for journal Atmos. Meas. Tech.
Discussion started: 9 June 2017

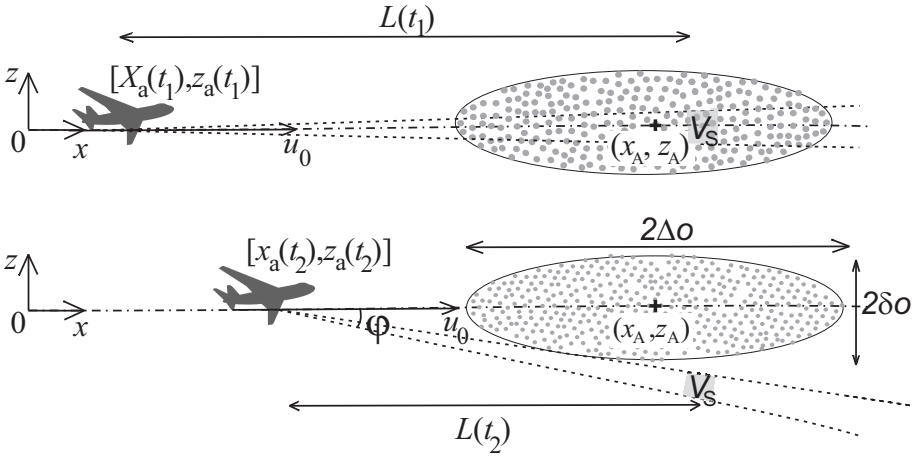

Figure 1. A schematic diagram of lidar measurements of the flight direction from an aircraft. The $x_a(t)$, $z_a(t)$ represent the observer's coordinates at sequential time points t_1 and t_2; the center of the observed clusters is marked with +, and their coordinates are x_A, z_A.

The position of the aircraft is defined by three angles: roll, yaw and pitch. As the horizontal size of typical aerosol formations is usually large, the azimuthal shifts of the scattering volume due to rolling and yawing are not as significant as its vertical shift, which is characterized by the product of the observation distance L and pitch angle change. Although the use of conventional gyro-stabilized platforms partially compensates for the fluctuations of the aircraft position, the residual angular deviation in the vertical angle still remains to be 0.3 to 0.6 degrees for conventional civil aircraft gyro-platforms (SOMAG AG Jena, 2016; Temp-Avia, 2016). At an observation distance of 16 kilometers, the shift of scattering volume due to such angle variations reaches about 83-168 meters in the vertical direction. For aerosol clusters with the thickness smaller or comparable to the shift of scattering volume, an incidental time modulation of the lidar response from monitored aerosol cluster may be mistaken for the cluster evolution.

Airborne lidar measurements in the flight direction, conducted in the DELICAT project (Huffaker and Hardesty, 1996; Inokuchi et al., 2009; Veerman et al., 2014) suggest that it may be possible to observe aerosol clusters with evolution time smaller than that of the measurement time interval. At the same time, such variations of the lidar response (Veerman et al., 2014, fig 22) could also be caused by variations of the airplane pitch. In this paper, we simulate and discuss the influence of airplane pitch angle variation on the lidar imaging of aerosol clusters.

It is evident that the backscattered signal coming from the aerosol, changes with pitch fluctuations. The scheme in Fig.1 shows that if the vertical shift of the scattering volume is large $L\sin(\varphi) > \delta o$, where L is the distance between the plane and the scattering volume, φ is the angle deflection of the sensing beam from flight direction, δo is the characteristic vertical size of the aerosol cluster, then the signal from long-living cluster contains distortions caused by scattering volume shift. These distortions may be mistaken for a result of the cluster evolution. The condition $L\sin(\varphi)/\delta o < 1$ is, therefore, a technical requirement ensuring the compensation for the beam deflection in order to suppress the noise caused by the pitch angle variations.

Atmos. Meas. Tech. Discuss., https://doi.org/10.5194/amt-2017-132
Manuscript under review for journal Atmos. Meas. Tech.
Discussion started: 9 June 2017

Atmospheric Measurement Techniques Discussions

If $L\sin(\varphi)/\delta o \geq 1$, then the aerosol cluster may occasionally disappear from the lidar's field of vision. Figure 1 is a schematic representation of the measurements with an airborne lidar that approaches a cluster (depicted by circlets) located on the flight path, with the airspeed u_0. The cluster thickness $2\delta o$ is much smaller than its horizontal dimension, $2\Delta o$. The flight path is shown by the dash-and-dot line. The laser beam is shown by the long-dash line. The scattering volume V_S, which moves with the velocity of light c in measurement direction, is colored gray here. The scheme depicts two sequential time moments of measurements. In the second time moment, the beam deflects from the flight direction by angle φ and the lidar only registers molecular scattering at the thermodynamic fluctuations of the air density.

The following typical scales of time and distance may be distinguished in the problem of lidar monitoring of the atmosphere from an aircraft in the flight direction. Assuming that the molecular scattering is weak and neglecting the molecular absorption, we may accept the length of molecular extinction as the maximum distance scale L_{ext}. The intensity I of the observed backscatter response is decreases with the distance as L^{-2}. Together with the sensing pulse magnitude, the internal noises of the receiver, as well as the random nature of aerosol and turbulence determine the maximum sensing distance L_{max}. We assume that $L_{max} < L_{ext}$. The minimum time scale is the sensing pulse duration τ, which is about 10 nanoseconds for lasers used in lidars. The lengthwise dimension $l_{\|}$ of the scattering volume V_S equals $c\tau/2$, where c is the light speed. At $\tau = 10$ ns, which is typical for modern lidars, $l_{\|} = 1.5$ m. The lateral dimension $l_{\perp}$ is determined by the initial diameter D_0 of the sensing beam and divergence angle γ: $l_{\perp} \simeq \gamma L + D_0$. For the typical values of $\gamma = 2 \cdot 10^{-4}$ rad, $D_0 = 10$ cm, and $L_{max} = 15$ km, the estimated value of $l_{\perp}$ is about 3.1 m at the end of the sensing path. Signal record time is determined by the pass band of the photodetector and is usually slightly greater than τ. Another characteristic time is the time interval $t_{max} = 2L_{max}/c$ of backscatter return. It determines the maximum frequency of sensing pulses. For distances of, e.g., $L_{max} = 15$ km, the value of t_{max} is about 0.1 milliseconds. Such a time interval is negligible compared to the time scale of detectable variations in atmospheric aerosol systems (Ivlev and Dovgalyuk, 1999). For this reason, the properties of the scattering medium, including the aerosol density and backscattering cross-section, are considered to be invariant at time intervals t_{max} when analyzing the effects of cluster evolution upon lidar images.

Lidars, in most practical cases, send recurrent pulses. In Fig. 2 they are seen as a "comb". Because the shot frequency is taken to be less than $1/t_{max}$, we may use the approximation of delta-pulses, assuming, therefore, the backscattered signals to be independent for each pulse. In the hierarchy of characteristic times, the value of $t_{obs} = L_{max}/u_0$ is the time for the aircraft to approach the scatterer after the moment of its observation. The value of t_{obs} has been used in (Gurvich and Kulikov, 2016) to define long-living clusters. For observation distances from 10 to 20 km and modern aircraft velocities, this time may reach hundreds of seconds. The backscattering cross-section of aerosol particles may change significantly over the time interval of t_{obs}. This change is schematically depicted at Fig. 1 by the change in the number and size of scatterers.

3 Modeling of an aerosol cluster lidar image

For the lidar image model, we use a Cartesian coordinate system with its Ox axis coinciding with the flight direction of the aircraft moving straightforward at a constant altitude. We discuss relatively small distances, $\ll \sqrt{a_E H_A}$ where a_E is Earth

Atmos. Meas. Tech. Discuss., https://doi.org/10.5194/amt-2017-132
Manuscript under review for journal Atmos. Meas. Tech.
Discussion started: 9 June 2017

Atmospheric Measurement Techniques Discussions

radius, H_A is atmospheric scale height. Therefore, the Earth's curvature impact can be neglected. The coordinate system origin is placed somewhere on the flight path; the Oz axis is directed along the local vertical. Let's denote the aircraft position at time point t as $x_a(t) = u_0 \cdot t$, $z_a(t)$.

To investigate possible artifacts generated by uncontrolled wanderings of the line of sight, which may be caused, e.g., by the fluctuations of the aircraft position, errors in the beam stabilizing system, etc., we should consider the apparent movements of the scattering volume resulting from the above factors. If the distance between the aircraft and the center of the scattering volume at time t is L, then the coordinates x_S, z_S of the scattering volume center are:

$$x_S(t) = x_a(t) + L \cdot cos(\varphi(t)) \cong x_a(t) + L, z_S(t) = z_a(t) + L \cdot \sin(\varphi(t)) \cong L \cdot \varphi(t) \quad (1)$$

Backscattered radiation is detected with the delay

$$\delta t = 2L/c \quad (2)$$

after time t_0 when the sensing pulse was sent. Equation (2) allows the derivation of L from measured δt. Because the light velocity significantly exceeds the aircraft velocity, for the simulation purposes, it is conveniet to treat $L(t)$ and t, which can both be measured directly, as independent variables.

Below, we perform the analysis of the backscatter signal intensity $I(L,t)$ in the receiving aperture superimposed on the lidar output aperture. We apply the approximation of the single-scattering on aerosol particles (Ishimaru, 1978). We use the following notations: $\rho_A(x,y,z,t)$ is the number of scatterers per volume unit, or the scatterer density, and $\sigma_{AB}(x,y,z,t)$ is the aerosol differential backscatter cross-section coefficient. For an arbitrary shaped sensing pulse with its complex envelope $U(t,t_0)$, where t_0 is a time moment of pulse generation, the intensity registered by the receiver at an arbitrary time point is determined by the expression (Ishimaru, 1978, Eq. 5.35):

$$I(L,t) = Cs \int_{R_1}^{R_2} \frac{\rho(R',(t-t_0) - R'/c)\sigma_B(R',t-R'/c)}{R_2} |U_i(t-R'/c,t_0)|^2 e^{-2\Gamma(R',t)} dR' \quad (3)$$

Here $R_1 = c(t-t_0)/2$ and $R_2 = c(t-t_0+\tau)/2$ are the corresponding positions of the scattering volume boundaries, t_0 is the time of sensing pulse generation and $L = (R_1+R_2)/2$ is the position of the scattering volume center along the flight route. The integration is performed along the line of sight taking into account its direction fluctuations. The factor of $exp[-2\Gamma(R,t)]$ in (3) describes the extinction and is defined by equation

$$\Gamma(R,t) = Cd \int_{x_a(t)}^{R+x_a(t)} \rho(R',t-R'/c)\sigma_T(R',t-R'/c)dR' \quad (4)$$

Here, σ_T is total cross-section coefficient of scattering. The product of $\rho(R',t-R'/c)\sigma_T(R',t-R'/c)dR'$ describes the total losses from molecular and aerosol scatters. Constant factors Cs and Cd in front of the integrals in Eqs. (3) and (4) account for the sensing pulse energy, beam geometry, receiver aperture, detector parameters etc. Equation (3) does not take into account the

Atmos. Meas. Tech. Discuss., https://doi.org/10.5194/amt-2017-132
Manuscript under review for journal Atmos. Meas. Tech.
Discussion started: 9 June 2017

Atmospheric Measurement Techniques Discussions

contribution of weak molecular scattering, which, when the measured intensity $I(L,t)$ is multiplied by $L^2 exp(2\cdot\Gamma)$, generates a constant background on the lidar image obtained.

Because both the sensing pulse and detection time are very short as compared to typical times of atmospheric processes, the pulse may be approximated with a δ-function. Under this approximation, in the absence of measurement direction oscillations, signal $I(L,t)$ in receiver aperture is determined by the equation:

$$
\begin{aligned}
&I(L,t) = I_M(L,t) + I_A(L,t)\\
&I_M(L,t) = \frac{2C\cdot E_0}{c\cdot L^2}\rho_M(L,t-L/c)\sigma_{MB}(L,t-L/c)e^{-2\Gamma(L,t)}\\
&I_A(L,t) = \frac{2C\cdot E_0}{c\cdot L^2}\rho_A(L,t-L/c)\sigma_{AB}(L,t-L/c)e^{-2\Gamma(L,t)}
\end{aligned}
\tag{5}
$$

where the observed intensity I has two components, I_M, resulting from the molecular scattering, and I_A coming from the aerosol scattering. Here, E_0 is the pulse total energy, C is the normalizing factor that accounts for the sensing pulse shape, the receiver aperture, detector features etc., L is the distance between the lidar and the scattering volume. Equations (4) and (5) contain terms $\rho_M(R',t)\sigma_{MB}(R',t)$ and $\rho_A(R',t)\sigma_{AB}(R',t)$, which are the products of scatterers density by the cross-sections of the molecular and aerosol backscattering, respectively. The term $exp(-2\Gamma(L,t))$ describes extinction, $\rho(R',t-R'/c)\sigma_T(R',t-R'/c)dR'$ represents the total losses due to molecular and aerosol extinction. This relatively simple model appears to be a good approximation for a sensing laser pulse with the duration of several nanoseconds. The typical value of $\rho_M\sigma_{MB}$ for the weak aerosol (concentration 10^8 particles per m^{-3}, and density of water 49 $\mu\mathrm{g}/\mathrm{m}^{-3}$) is about $\rho_M\sigma_{MB} = 2\cdot 10^{-2}$ dB/km (Ishimaru, 1978). For the simulation purposes, we use the following normalized function for the atmospheric aerosol backscattering density:

$$
\mathrm{P(x,z,t)} = \rho_M\sigma_{MB}(x,y,z,t)/\rho_M\sigma_{MB}(max) = a\sum\nolimits_q exp[-(\tfrac{x-x_{0q}}{\Delta o_q})^4 - (\tfrac{y}{\Delta y_q})^4 - (\tfrac{z-z_{0q}}{\delta o_q})^2 - (\tfrac{t-t_q}{\Delta t_q})^2]
\tag{6}
$$

Table 1. Parameters of aerosol clusters

Cluster	Δo_q, km	Δt_q, sec	x_{0q},km	t_q,sec	$u_0 t_{obs}/\Delta o_q$
A	2.0	60	11.0	34	5.1
B	1.0	40	16.3	70	6.8
C	1.0	40	20.0	40	6.8
D	1.0	16	24.0	80	2.7
E	0.5	10	28.0	95	3.4

In this expression, x is the axis collinear to the flight direction, y is the axis perpendicular to both the flight direction and vertical axis, z is the vertical axis, orthogonal to the Earth's surface below the aircraft position, t is the moment of measurement, which we assume to coincide with the moment of pulse pulse generation t_0, due to the aforementioned smallness of the ratio

Atmos. Meas. Tech. Discuss., https://doi.org/10.5194/amt-2017-132
Manuscript under review for journal Atmos. Meas. Tech.
Discussion started: 9 June 2017

Atmospheric Measurement Techniques Discussions

$L_{max}/(c\cdot\Delta t_q)\ll 1$, x_{0q}, y_{0q} and z_{0q} are coordinates of the clusters' centers, t_q is the time moment of the maximum cluster density, Δt_q is the typical cluster evolution time, Δo_q is the cluster scale in the flight direction, δo_q is the typical vertical dimension of cluster. The value of Δy_q is the transverse size of the cluster. The contribution of fluctuations of the flight direction along y-axis into the lidar image noise is neglegible, because the changes of scatterers' density are smooth. The parameter Δy_q is chosen to equal Δo_q for all the simulated clusters. The sequence of five integers q, from 1 to 5, is the sequence order of clusters along the flight path. The model parameters are summarized in the Table 1. All the five clusters have the same thickness $2\delta o_q = 2\delta o$, which was equal to $100\mathrm{m}; 300\mathrm{m}; 900\mathrm{m}$ in different simulations. Figure 2 presents the cluster sequence used in the model for $\delta o = 150\mathrm{m}$. Aerosol cluster are represented as surfaces calculated at e^{-1} level of values. The distance from the initial position of the aircraft is laid off along the Ox axis, the flight altitude is laid off along the Oz axis and time along the t axis. The aircraft velocity is assumed to be 170 $\mathrm{m/sec}$.

The last column of the table contains the unitless ratios $u_0\cdot t_{obs}/\Delta o_q$. Because all of them are greater than 1, we can consider our modeled clusters as long-living ones (Gurvich and Kulikov, 2016). We consider "thin" clusters, whose ratios of vertical scales to lengthwise ones are $\delta o/\Delta o \ll 1$. If such clusters are detected in the vertical direction from a ground-based platform, they are registered as layers in the altitudinal distribution of the aerosol.

Since our work is aimed at the study of the most typical features of the cluster image changes, we only discuss their shape and relative size, without focusing on the type of particles that produce the signal. Consequently, the value we need to monitor is the normalized backscatter intensity $J_A(L,t) = [I_A(L,t)]/I_M(L,t)$. As the constant background coming from the scattering on density inhomogeneities does not present any interest the lidar images, all the Figures present the value of $J_A(L,t)$.

Fig. 3 shows the lidar image of aerosol clusters, modeled according to model (6). This image is simulated under the assumption of the stable flight altitude and measurement direction. In terms of Eq. (1), this means that $\varphi = 0$ and $z_S = const$, the latter value may be set to the flight altitude without restricting the generality. We focus on the problem of the impact of flight parameter fluctuations upon measured lidar backscattered signal. The experiment discussed in (Veerman et al., 2014, Introduction) was conducted under clear air conditions. For this reason, for our numerical simulation, we choose the product of scatterer cross-section and density $\rho_M\sigma_{MB}$ to be equal to $2\cdot 10^{-2}$ $\mathrm{dB/km}$ at the cluster's center. This value typically corresponds to weak aerosol clusters in accordance with Fabelinskii (2012); Ishimaru (1978), which implies that the aerosol scattering does not significantly decrease the propagating laser pulse energy.

The image J_A at Fig. 3 is shown in $(L, u_0 t)$ coordinates, in which the cluster with a lifespan of $\Delta t > L_{max}/u_0$ looks like a bar, whose slope with respect to the OL axis equals $\pi/4$. Longitudinal cluster scale Δo determines the image size along the L axis. Vertical cluster scale does not influence the lidar image under the assumed conditions. The image size at an angle of $-\pi/4$ with respect to the L axis, is determined by $u_0\Delta t_q$ i.e. the product of aircraft speed by cluster's lifespan. Measurement of the image length J_A along this direction allows, therefore, the estimation of the cluster lifespan Δt_q. This parameter is important for obtaining images of short-living clusters at large distances L, because the observer moves closer to the detected cluster. If the cluster has a long lifespan, such that $u_0\Delta t_q \gg L_{max}$, then, for a constant measurement direction, its lidar image is a homogeneous bar.

Atmos. Meas. Tech. Discuss., https://doi.org/10.5194/amt-2017-132
Manuscript under review for journal Atmos. Meas. Tech.
Discussion started: 9 June 2017

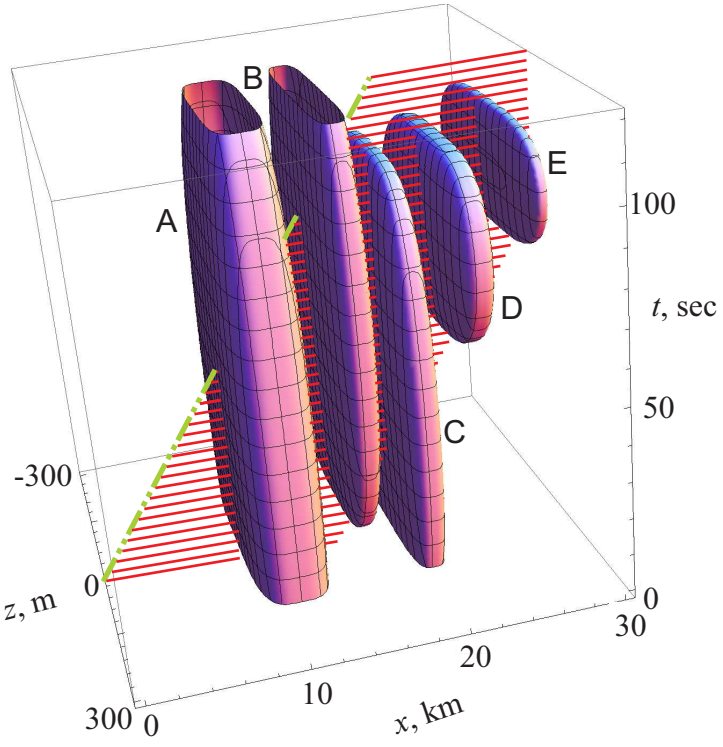

Figure 2. 3D images of aerosol clusters $P(x,z,t)$, calculated at $1/e$ level, for the model given by eq.(6). Dash-and-dot line is the flight trace, red "comb" represents sensing laser pulses, $L_{max} = 16$ km, $\varphi_0 = 0$.

4 The impact of measurement direction fluctuations on cluster lidar images

Under the real-world conditions, the uncontrolled variations of measurement directions always exist due to both vibrations of the carrying platform and fluctuations of flying aircraft position. If a cluster is strongly elongated in horizontal direction, then its lidar image is most sensitive to vertical variations of the measurement direction. For the simulation of the effects caused by sensing beam deviation from the flight direction, we assume that the measurement direction, which is determined in (1) by the angle φ, changes periodically with a period of $T_\varphi = 20$ sec according to the equation

$$\varphi(t) = \varphi_0 \cdot [2\pi u_0 t / T_\varphi] \tag{7}$$

where the normalization factor of φ_0 determines the maximum deviation angle from the flight direction. Given the precision characteristics of modern gyro-stabilizing devices used in civil aviation (Temp-Avia, 2016; SOMAG AG Jena, 2016), we consider here two φ_0 values: $\varphi_0 = 3$ and $\varphi_0 = 6$ degrees. We consider here $z_a(t) = 0$.

The aircraft position fluctuations result in fluctuations of the center of scattering value $z_S(t)$ at the same distance, without causing new type of effects compared to the angle fluctuations. Fig. 4 shows the relation between the deviation of the scattering

Atmos. Meas. Tech. Discuss., https://doi.org/10.5194/amt-2017-132
Manuscript under review for journal Atmos. Meas. Tech.
Discussion started: 9 June 2017

Atmospheric Measurement Techniques Discussions

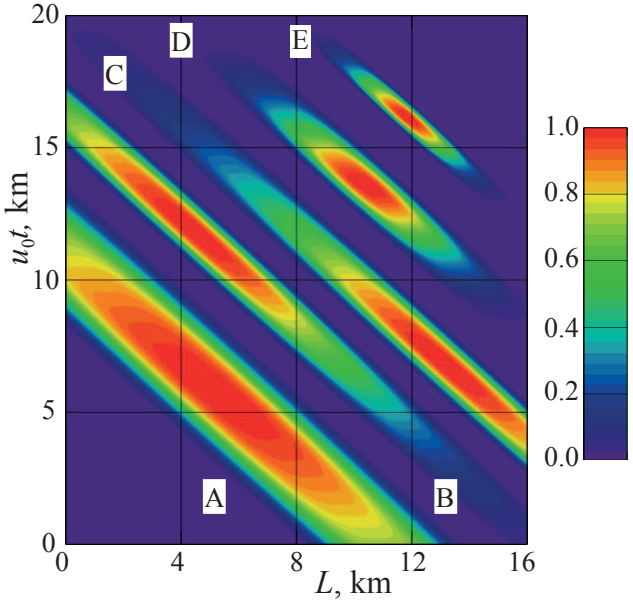

Figure 3. Lidar images $J_A(L,t)$ of aerosol clusters simulated according to the model (eq. (6)) for a constant beam direction aligned with the flight trace. The scale of J_A is given in pseudo-color at the left. The vertical axis corresponds to the product of u_0t_0 where t_0 is a sensing pulse generation point and u_0 is the aircraft speed.

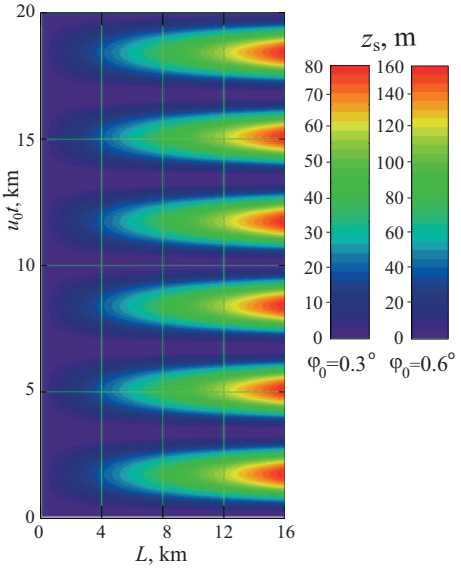

Figure 4. Deviation z_S of the scattering volume center from the flight direction as a function of the pulse generation time t and of the distance L.

Atmos. Meas. Tech. Discuss., https://doi.org/10.5194/amt-2017-132
Manuscript under review for journal Atmos. Meas. Tech.
Discussion started: 9 June 2017

Atmospheric Measurement Techniques Discussions

volume center coordinate $z_S = L \cdot \varphi(t)$, the measurement time $u_0 t$ and the distance L between the observer and the scattering volume center.

Vertical movements of the scattering volume center z_S comparable to or greater than z_S should be visible in the lidar image. This qualitatively follows from the description of the measurement setup in Section 2. Lidar images computed in the presence of pitch angle fluctuations are presented in Fig. 5.

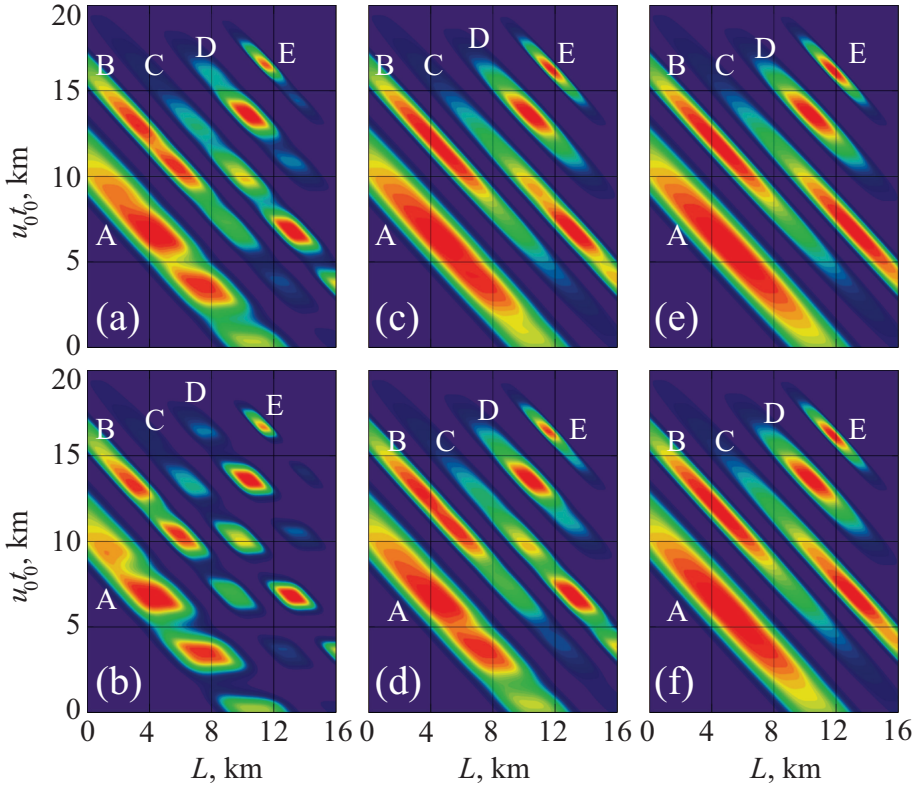

Figure 5. The impact of measurement direction fluctuations on the lidar image J_A of aerosol clusters. The pseudo-colored scale of J_A values is the same as in Fig. 3. Panes: (a), (c), (e) - oscillations amplitude $\varphi_0 = 0.3$degrees, panes: - (b), (d), (f) - $\varphi_0 = 0.6$degrees; panes: (a), (b) vertical dimension $\delta o = 50$ m, panes: (c), (d) - $\delta o = 150$ m, panes: (e), (f) - $\delta o = 450$ m.

The same 5 aerosol clusters described by Eq. (6) and shown in Fig.2 are taken for lidar image simulations, but their δo parameters that determine vertical dimensions are set to different values. Panes (a), (c) and (e) grouped in the upper row show the images simulated at lower oscillation amplitude $\varphi_0 = 0.3$ degree, for δo values of 50, 150 and 450 m. The images at lower row panes: (b), (d) and (f), have a twice higher amplitude $\varphi_0 = 0.6$ degrees and the same values, respectively. The measurement time is 120 sec for each pane and the maximum measurement distance $L_{max} = 16$ km. Since the maximum vertical deviations of the scattering volume center coordinate z_S from the flight path reach 83 m and 168 m, respectively, it is possible to consider cases with $z_S > \delta o$ and $z_S < \delta o$.

Atmos. Meas. Tech. Discuss., https://doi.org/10.5194/amt-2017-132
Manuscript under review for journal Atmos. Meas. Tech.
Discussion started: 9 June 2017

Atmospheric Measurement Techniques Discussions

The comparison of the Fig. 3 and Fig. 5 reveals that sensing direction oscillations cause breaches in the clusters lidar images at large distances L when the deviations of z_S reach the maximum values. These signal fades appear due to the scattering volume shift outside cluster boundaries; the maximal shift equals $\varphi_0 L$. For this reason the images are more distorted at the right side of each pane of Fig. 5. Image distortions are more intense for thin clusters with low values of δo.

Fig.5 (a), (b) shows that the breaches appear at the same aircraft position $u_0 t_0$ for all clusters. The lines could be drawn at 2 km, 5 km (as well as at 8, 12, 15, and 18 km) in accordance with the beam direction variations. The value of $\varphi_0 L$ is smaller for smaller distance L, consequently, the breaches "depth" is smaller for a close distance. Thus the angle φ_0 could be estimated from the intensity measurements. It may be expected that a natural process intensity, like aerosol evolution due to evaporation or condensation, varies for different clusters. A distortion due to flight direction fluctuations has the same impact on the images of all the clusters observed at the same distance.

For thickness values large enough, like in panes (e) and (f), the images almost do not differ from the images in Fig. 3 computed with zero φ_0 value, i.e. in the absence of measurement direction oscillations. Therefore, if the condition $z_S \ll \delta o$ is fulfilled, the cluster layers can be reconstructed by lidar measurements.

The data presented in Fig. 5 also suggest the possibility of obtaining actual information about the vertical structure of the aerosol cluster from measurements of $\varphi(t)$ in flight.

5 Airborne lidar measurements in presence of pitch angle fluctuations

We consider the results of the airborne measurements carried out in the framework of DELICAT project (Veerman et al., 2014, flight map Fig.15). Laboratory of Turbulence and Wave Propagation at Obukhov Institute of Atmospheric Physics was one of the participants of the DELICAT project. The DELICAT airborne lidar is based on a high-power Nd:YAG laser, which generates 7.7 ns length pulses at wavelength 1064 nm. The third garmonic ($\lambda = 355$ nm) with energy about 80 mJ was used for ahead sensing. The angular beam divergence was about of 200 μrad. Lidar receiver contained several subsystems such as telescope with 140 mm diameter, and optical components for filtering, beam forming, stabilization, and detection. The receiver had two channels: for co- and cross-polarization. Lidar range resolution was about 5 m. Further details of the experimental setup can be found in (Veerman et al., 2014).

In this paper, we only consider the co-polarized component. For the case that we discuss below, it only differs from the cross-polarized component by the amlitude coefficient. The flight routes for the DELICAT experiments were chosen in order to avoid large amount of aerosol. Usual civil aircraft flight can include much more aerosol clouds. The measured intensity is normalized in order to compensate the signal decay with the distance $I(L,t)_{norm} = I(L,t) * (R/R_{2km})^2$ and presented in Fig.6.

We only present a few minutes of flight N9 measured in France, August 8, 2013. The measurements presented in Fig.6a were acquired during the time interval from 8.32 pm to 8.33 pm UTC time, between the geographical lattitude/longitude positions (47.200352,6.488001) and (47.307705,6.485252) at a height of $10\mathrm{km}$. The measurements presented in Fig.6b were acquired during the time interval from 8.22 pm to 8.23 pm UTC time, between the geographical positions (46.262356,6.375160) and

Atmos. Meas. Tech. Discuss., https://doi.org/10.5194/amt-2017-132
Manuscript under review for journal Atmos. Meas. Tech.
Discussion started: 9 June 2017

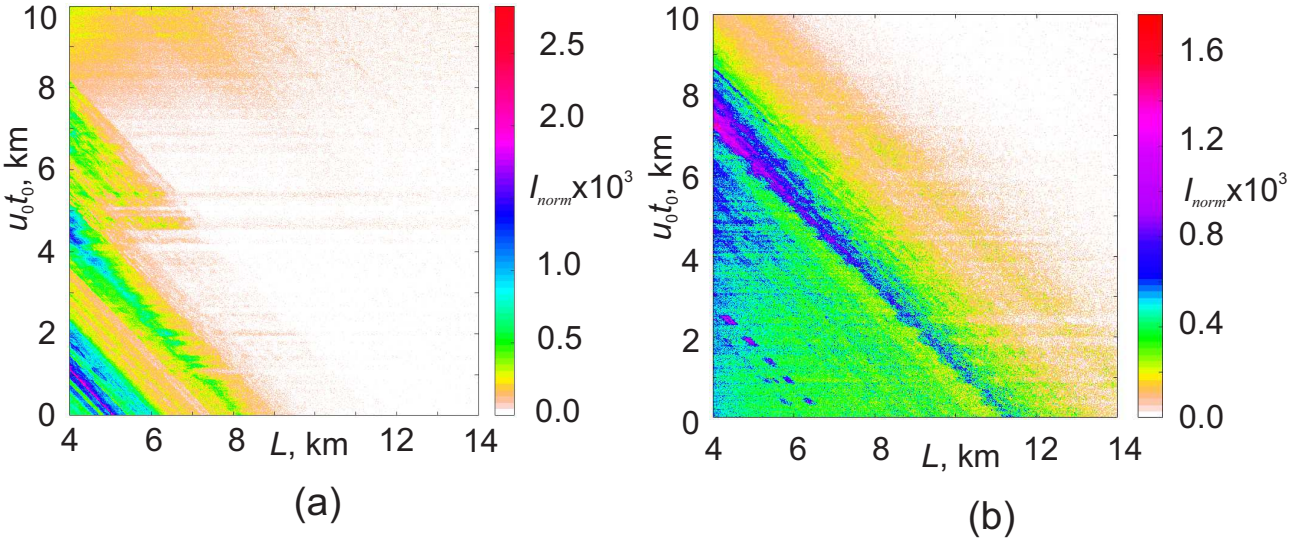

Figure 6. The normalized intensity I_{norm} measured during 1 minute at airborne experiments (a) without noticiable fluctuations of flight parameters; (b) in presence of pitch angle fluctuations.

(46.327354,6.483657) at a height of 9.46 km. The aircraft speed was about of $170\mathrm{m/s}$ in both cases. The backsckattered signal contains noise caused by different sources. Since this paper is mostly devoted to pitch angle fluctuations, we consider experimental data in the areas of the observation distance from 4 km to 14 km, which are almost free from the other noise factors. The signal almost without breaches is presented in Fig.6a. In this case, there is no pitch angle fluctuations and the aerosol cluster appears as a bar in the left bottom corner. The pitch angle fluctuations lead to breaches in the lidar signal. At least three aerosol clusters can be found at the Fig.6b. The first two clusters, firstly detected at distances 6 km and 6.5 km, respectively, are weak.

The third cluster, firstly detected at 11.5 km distance, has a larger scale size along the flight direction. It must also have a larger vertical scale, because it reacts on the picth angle variation weaker than the other clusters. The breaches appear in all the clusters at the same time, which means that they may result from the pitch angle variations. The normalized intensity of aerosol cluster reflections decreases with the distance. It may result from the scattering on aerosol particles. It also clear that such decreasing is only observed for large aerosol clusters.

6 Conclusions

In this paper the influence of fluctuations of the flight parameters upon images acquired by an airborne lidar system sensing ahead of the aircraft along the flight direction have been discussed in regard to the dependence on characteristic sizes of aerosol layers. It is shown that the pitch angle fluctuations are the most important factor for the discussed airborne lidar sensing scenario. We performed numerical simulations, which demonstrate the pitch angle fluctuation impact upon lidar images. The

Atmos. Meas. Tech. Discuss., https://doi.org/10.5194/amt-2017-132
Manuscript under review for journal Atmos. Meas. Tech.
Discussion started: 9 June 2017

simulations cover the thicknesses of atmospheric aerosol clusters in the range of tens and hundreds of meters accounting for realistic values of pitch angle fluctuations. We also show that LIDAR sensing ahead along the flight direction can potentially provide information about aerosol temporal evolution characteristics. We demonstrate that pitch angle fluctuations can have a noticeable impact upon measurements of the backscattered signal, even for a lidar system mounted on a stabilizing gyro-platform. Numerical simulations predict that uncontrolled fluctuations can result in signal noise including extreme fades and spikes. We show that the aerosol concentration variations on a scale of 100-300 m have a significant impact on the backscattered signal, if the correction for the angular fluctuation has a residual rms error about of 0.1–0.2 degrees, which is typical for conventional gyro-platforms used in the civil aviation. Fluctuation influence is shown to depend on the characteristic vertical size of atmospheric aerosol clusters and to introduce larder errors for aerosol variations on smaller vertical scales. We formulate criteria for distinguishing this impact from the temporal evolution of atmospheric aerosol clouds. We presented and discussed an example of airborne lidar experimental observations from the DELICAT project that shows signal variations simultaneously appearing from different aerosol clusters consistent with the signal fades caused by the impact of pitch angle fluctuations in accordance with our simulations.

Acknowledgements. The authors are grateful to M.E. Gorbunov and A.V. Shmakov for fruitful discussions, O.V. Fedorova for the thorough manuscript review, and F. Dalaudier for turning our attention to the significance of measurement direction control. Work on Sections 1-3 was supported by the Russian Science Foundation (grant RSCF No. 14-27-00134). Work on Sections 4 and 5 was supported by Russian Foundation for Basic Research (grant No. 16-05-00358-a).

References

Acharya, Y.B., Sharma, S. and Chandra, H.: Signal induced noise in PMT detection of lidar signals, Measurement, 35(3), 269-276, 2004.

Barenblatt, G. I., and Monin, A. S.: Similarity laws for turbulent stratified shear flows, Archive for Rational Mechanics and Analysis, 70, 307 - 317, 1979.

Bohren, C. F., and Huffman, D. R.: Absorption and scattering of light by small particles, John Wiley & Sons, 530 p., 2008.

Burton, S.P., Hair, J.W., Kahnert, M., Ferrare, R.A., Hostetler, C.A., Cook, A.L., Harper, D.B., Berkoff, T.A., Seaman, S.T., Collins, J.E. and Fenn, M.A.: Observations of the spectral dependence of linear particle depolarization ratio of aerosols using NASA Langley airborne High Spectral Resolution Lidar, Atmospheric Chemistry and Physics, 15(23), 13453-13473, 2015.

Burton, S.P., Vaughan, M.A., Ferrare, R.A. and Hostetler, C.A.: Separating mixtures of aerosol types in airborne High Spectral Resolution Lidar data, Atmospheric Measurement Techniques, 7(2), 419-436, 2014.

Cadet, B., Giraud, V., Haeffelin, M., Keckhut, P., Rechou, A. and Baldy, S.: Improved retrievals of the optical properties of cirrus clouds by a combination of lidar methods. Applied optics, 44(9),1726-1734, 2005.

Chazette, P., Dabas, A., Sanak, J., Lardier, M. and Royer, P.: French airborne lidar measurements for Eyjafjallajökull ash plume survey, Atmospheric Chemistry and Physics, 12(15), 7059-7072, 2012.

Dacre, H.F., Grant, A.L. and Johnson, B.T.: Aircraft observations and model simulations of concentration and particle size distribution in the Eyjafjallajökull volcanic ash cloud, Atmospheric Chemistry and Physics, 13(3), 1277-1291, 2013.

Fabelinskii, I. L.: Molecular scattering of light, Springer Science & Business Media, 622 p., 2012.

Godbaz, J.P., Cree, M.J. and Dorrington, A.A.: Closed-form inverses for the mixed pixel/multipath interference problem in amcw lidar, In IS&T/SPIE Electronic Imaging, 829618-829618, 2012.

Gurvich, A. S., and Kulikov V. A.: Lidar sensing of the turbulence based on the backscattering enhancement effect, SPIE LASE, Free-Space Laser Communication and Atmospheric Propagation XXV, pp. 86100U-86100U, International Society for Optics and Photonics, 2013.

Gurvich, A. S., and Kulikov, V. A.: Airborne Lidar sounding of short-lived aerosol clusters, Atmospheric and Oceanic Optics, 29, 410 - 414, doi:10.1134/S1024856016050079, 2016.

Haarig, M., Engelmann, R., Ansmann, A., Veselovskii, I., Whiteman, D. N., and Althausen, D.: 1064 nm rotational Raman lidar for particle extinction and lidar-ratio profiling: cirrus case study, Atmospheric Measurement Techhniques, 9, 4269 - 4278, doi:10.5194/amt-9-4269-2016, 2016.

Hair, J.W., Hostetler, C.A., Cook, A.L., Harper, D.B., Ferrare, R.A., Mack, T.L., Welch, W., Izquierdo, L.R. and Hovis, F.E.: Airborne high spectral resolution lidar for profiling aerosol optical properties, Applied optics, 47(36), 6734-6752, 2008.

Hauchecorne, A., Cot, C., Dalaudier, F., Porteneuve, J., Gaudo, T., Wilson, R., Cenac, C., Laqui, C., Keckhut, P., Perrin, J. M., and Dolfi, A.: Tentative detection of clear-air turbulence using a ground-based Rayleigh lidar, Applied Optics, 55, 3420 - 3428, doi:10.1364/AO.55.003420, 2016.

Hervo, M., Quennehen, B., Kristiansen, N.I., Boulon, J., Stohl, A., Fréville, P., Pichon, J.M., Picard, D., Labazuy, P., Gouhier, M. and Roger, J.C.: Physical and optical properties of 2010 Eyjafjallajökull volcanic eruption aerosol: ground-based, Lidar and airborne measurements in France. Atmospheric Chemistry and Physics, 12(4), 1721-1736, 2012.

Hoareau, C., Keckhut, P., Baray, J. L., Robert, L., Courcoux Y., Porteneuve J., Vomel H., and Morel, B.: A Raman lidar at La Reunion (20.8 S, 55.5 E) for monitoring water vapor and cirrus distributions in the subtropical upper troposphere: preliminary analyses and description of a future system, Atmospheric Measurement Techhniques, 5, 1333 - 1348, doi:10.5194/amt-5-1333-2012, 2012.

Huffaker, R. M., and Hardesty, R. M.: Remote sensing of atmospheric wind velocities using solid-state and CO2 coherent laser systems, Proceedings of the IEEE, 84, 181-204, doi:10.1109/5.482228, 1996.

Inokuchi, H., Endo, E., Ando, T., Asaka, K., Tanaka, H., and Hirano, Y.: Development of an airborne wind measurement system, International Symposium on Photoelectronic Detection and Imaging 2009: Laser Sensing and Imaging, edited by Farzin Amzajerdian, Chun-qing Gao, Tian-yu Xie, Proc. of SPIE Vol. 7382, 738205 doi: 10.1117/12.836606, 2009.

Inokuchi, H., Tanaka, H. and Ando, T.: Development of an onboard doppler lidar for flight safety, Journal of aircraft, 46(4), 1411-1415, 2009.

Ivlev, L. S., and Dovgalyuk, Y. A.: Physics of atmospheric aerosol systems, Saint-Petersburg State University, 188 p., 1999.

Ishimaru A.: Wave propagation and scattering in random media, Academic press NY, 572 p, 1978.

Jentink, H.W. and Bogue, R.K., Optical air flow measurements for flight tests and flight testing optical air flow meters, In Flight Test – Sharing Knowledge and Experience, Meeting Proceedings RTO-MP-SCI-162, Paper 11, France, 2005.

Johnson, B., Turnbull, K., Brown, P., Burgess, R., Dorsey, J., Baran, A.J., Webster, H., Haywood, J., Cotton, R., Ulanowski, Z. and Hesse, E.: In situ observations of volcanic ash clouds from the FAAM aircraft during the eruption of Eyjafjallajökull in 2010, Journal of Geophysical Research: Atmospheres, 117(D20), DOI: 10.1029/2011JD016760, 2012.

Kandidov, V.P., Shlenov, S.A. and Kosareva, O.G.G.E.: Filamentation of high-power femtosecond laser radiation. Quantum Electronics, 39(3), p.205-228 2009.

Keckhut, P., Courcoux, Y., Baray, J. L., Porteneuve, J., Veremes, H., Hauchecorne, A., Dionisi, D., Posny, F., Cammas, J. P., Payen G, Gabarrot F.: Introduction to the Maido Lidar Calibration dedicated to the validation of upper air meteorological parameters, Journal of Applied Remote Sensing, 9, 094099, doi:10.1117/1.JRS.9.094099, 2015.

Kiemle, C., Wirth, M., Fix, A., Ehret, G., Schumann, U., Gardiner, T., Schiller, C., Sitnikov, N. and Stiller, G., First airborne water vapor lidar measurements in the tropical upper troposphere and mid-latitudes lower stratosphere: accuracy evaluation and intercomparisons with other instruments. Atmospheric chemistry and physics, 8(17), 5245-5261, 2008.

Kleinman, L.I., Springston, S.R., Daum, P.H., Lee, Y.N., Nunnermacker, L.J., Senum, G.I., Wang, J., Weinstein-Lloyd, J., Alexander, M.L., Hubbe, J. and Ortega, J.: The time evolution of aerosol composition over the Mexico City plateau. Atmospheric Chemistry and Physics, 8(6), 1559-1575, 2008.

Klyatskin, V. I.: Diffuse and clusterization of passive admixture in random hydrodynamic flows, Moscow Fizmatlit, 149 p., 2005.

Klyatskin, V. I., and Koshel, K. V.: Simple example of the development of cluster structure of a passive tracer field in random flows, Physics-Uspekhi 43, 717 - 723, doi:10.1070/PU2000v043n07ABEH000743, 2000.

Koch, S.E., Jamison, B.D., Lu, C., Smith, T.L., Tollerud, E.I., Girz, C., Wang, N., Lane, T.P., Shapiro, M.A., Parrish, D.D. and Cooper, O.R.: Turbulence and gravity waves within an upper-level front, Journal of the atmospheric sciences, 62(11), 3885-3908, 2005.

Kosareva, O.G., Murtazin, I.N., Panov, N.A., Savelev, A.B., Kandidov, V.P. and Chin, S.L.: Pulse shortening due to filamentation in transparent medium, Laser Physics Letters, 4(2), 126-132, 2006.

Lane, T.P., Sharman, R.D., Clark, T.L. and Hsu, H.M.: An investigation of turbulence generation mechanisms above deep convection, Journal of the atmospheric sciences, 60(10), 1297-1321, 2003.

Leblanc, T. and McDermid, I.S.: Accuracy of Raman lidar water vapor calibration and its applicability to long-term measurements. Applied optics, 47(30), 5592-5603, 2008.

Liu, Z.S., Wu, D., Liu, J.T., Zhang, K.L., Chen, W.B., Song, X.Q., Hair, J.W. and She, C.Y.: Low-altitude atmospheric wind measurement from the combined Mie and Rayleigh backscattering by Doppler lidar with an iodine filter, Applied optics, 41(33), 7079-7086, 2002.

Lu, C. and Koch, S.E.: Interaction of upper-tropospheric turbulence and gravity waves as obtained from spectral and structure function analyses, Journal of the Atmospheric Sciences, 65(8), 2676-2690, 2008.

Meng, Z. and Seinfeld, J.H.: Time scales to achieve atmospheric gas-aerosol equilibrium for volatile species, Atmospheric Environment, 30(16), 2889-2900, 1996.

Nappo, C.J.: An introduction to atmospheric gravity waves, Academic Press, 365 p., 2013.

Plougonven, R. and Zhang, F.: Gravity waves generated by jets and fronts and their relevance for clear-air turbulence, In Aviation Turbulence (pp. 385-406). Springer International Publishing, 2016.

Veerman, H. P. J., Vrancken, P., Lombard, L.: Flight testing delicat - a promise for medium-range clear air turbulence protection, European 46th SETP and 25th SFTE Symposium 2014, Lulea, Sweden, 2014.

Veselovskii, I., Whiteman, D. N., Korenskiy, M., Suvorina, A., and Perez-Ramirez, D.: Use of rotational Raman measurements in multi-wavelength aerosol lidar for evaluation of particle backscattering and extinction, Atmospheric Measurement Techhniques, 8, 4111 - 4122, doi:10.5194/amt-8-4111-2015, 2015.

Reichardt, J., Reichardt, S., Behrendt, A. and McGee, T.J.: Correlations among the optical properties of cirrus-cloud particles: Implications for spaceborne remote sensing, Geophysical research letters, 29(14), 2002.

Schmitt, N.P., Rehm, W., Pistner, T., Zeller, P., Diehl, H. and Nave, P.: The AWIATOR airborne LIDAR turbulence sensor, Aerospace Science and Technology, 11(7-8), 546-552, 2007.

Company SOMAG AG Jena, product GSM 3000 http://www.somag-ag.de/gsm-3000/

Targ, R., Steakley, B.C., Hawley, J.G., Ames, L.L., Forney, P., Swanson, D., Stone, R., Otto, R.G., Zarifis, V., Brockman, P. and Calloway, R.S.: Coherent lidar airborne wind sensor II: flight-test results at 2 and 10 μm. Applied optics, 35(36), 7117-7127, 1996.

Temp-Avia, product MGV-4V http://www.temp-avia.ru/index-13.htm

Thales Avionics and ONERA: A 1.5 μm LIDAR demonstrator of low airspeed measurement for civil helicopter, Proceedings of the 30th European Rotorcraft Forum, (2004).

Turnbull, K., Johnson, B., Marenco, F., Haywood, J., Minikin, A., Weinzierl, B., Schlager, H., Schumann, U., Leadbetter, S. and Woolley, A.: A case study of observations of volcanic ash from the Eyjafjallajökull eruption: 1. In situ airborne observations, Journal of Geophysical Research: Atmospheres, 117(D20), 2012.

Fritts, D.C. and Alexander, M.J.: Gravity wave dynamics and effects in the middle atmosphere, Reviews of geophysics, 41(1), 2003.

Fukuchi, T. and Shiina, T.: Industrial applications of laser remote sensing, Bentham Science Publishers, 2012.

Weitkamp, C.: Lidar: range-resolved optical remote sensing of the atmosphere, Springer Science & Business, 2006.

Whiteman, D.N., Melfi, S.H. and Ferrare, R.A.: Raman lidar system for the measurement of water vapor and aerosols in the Earth's atmosphere. Applied Optics, 31(16), 3068-3082, 1992.

Zuev, V. E., and Zuev, V. V.: Remote optical sensing of the atmosphere, Gidrometeoizdat, Moscow, 232 p., 1992.